DOI: 10.1002/cjoc.201300006

Morphology Control of Bi_2S_3 Nanostructures and the Formation Mechanism

HeeJin Kim,[a,b,+] Ji-eun Park,[b,+] Kyung Kim,[b] Mi-Kyung Han,*[,b] Sung-Jin Kim,*[,b] and Wooyoung Lee*[,a]

[a] *Department of Materials Science and Engineering, Yonsei University, Seoul 120-749, Korea*
[b] *Department of Chemistry and Nano Science, Ewha Womans University, Seoul 120-750, Korea*

Bismuthinite (Bi_2S_3) nanostructures were prepared by a hydrothermal method with sodium ethylenediaminetetraacetate (EDTA-Na_2). The morphology of Bi_2S_3 nanostructures was changed from a nanorod to a nanoplate by presence of the EDTA-Na_2. The altered morphology was caused by the capping effect of EDTA-Na_2 with Bi^{3+} ions, which induces the suboptimal growth direction due to partially blocking the preferential orientation direction. When the EDTA-Na_2/Bi^{3+} molar ratio＝1, the growth of Bi_2S_3 nanostructures was not allowed due to the chelating effect of EDTA-Na_2. The obtained Bi_2S_3 nanorods, stacked nanorods, nanoplates and nanoparticles were characterized using X-ray diffraction (XRD), transmission electron microscopy (TEM), high-resolution transmission electron microscopy (HRTEM) and selected area electron diffraction (SAED) pattern. A possible formation mechanism of these morphologies was proposed. The successful synthesis of various morphologies of nanostructured Bi_2S_3 may open up new possibilities for thermoelectric, electronic and optoelectronic uses of nanodevices based on Bi_2S_3 nanostructure.

Keywords bismuth sulfide (Bi_2S_3), hydrothermal, nanorod, nanoplate, thermoelectric material

Introduction

$A^V{}_2B^{VI}{}_3$ (A＝Sb, Bi, As; B＝S, Se, Te) group semiconductor compounds can be used in the applications of photoconducting targets, thermoelectric devices, electronic and optoelectronic devices, and infrared (IR) spectroscopy.[1] Especially, Bi_2S_3 is useful as a material for photodiode arrays and photovoltaic converters due to its direct band gap (E_g) of 1.3 eV.[2,3] Bi_2S_3 is also used as a thermoelectric cooling material based on the Peltier effect.[4] Recently, many reports in a variety of journals have focused on 1-dimensional (1D), 2-dimensional (2D), and 3-dimensional (3D) crystalline Bi_2S_3 using various methods, such as solvothermal and hydrothermal processes,[5-13] microwave synthesis,[14,15] thermal decomposition,[16-19] hot injection method,[20,21] template method,[22,23] single source precursor method,[24] and self-assembly method.[25-28]

Experimental conditions of solvothermal and hydrothermal processes, such as a sulfur source, solvent type, and surfactant are important factors for controlling the morphology of Bi_2S_3 nanostructures.[9-13] For example, ultralong nanoribbons have been obtained using an NaOH and glycerol solution,[9] nanotubes were obtained using octadecylamine,[10] nanoribbons were obtained using three kinds of characteristic sulfur sources ($Na_2S_2O_3$, elemental S and Na_2S),[11] superhydrophobic Bi_2S_3 complex nanostructures were obtained using biomolecules (tripeptide glutathione (γ-Glu-Cys-Gly)),[12] and 3D Bi_2S_3 matlike architectures composed of assembled nanorods were obtained using seeded substrate.[13]

Especially, 3D Bi_2S_3 structures composed of 2D Bi_2S_3 have been focused on various applications, such as a hydrogen storage, high-energy batteries, and catalytic fields due to their unique structure and high surface area.[29] Most of these 3D structures are constituted of 1D or 2D nanostructures. Because of this, the control of Bi_2S_3 1D and 2D morphologies is very important. But, the simple control of Bi_2S_3 morphology still remains difficult due to a lack of comprehension of the anisotropic properties in the Bi_2S_3 structure.

In this paper, we reported on the morphological change of the Bi_2S_3 nanostructures by changing the molar ratio of EDTA-Na_2/Bi^{3+} without changing the sulfur source, solvent type, and surfactant. A variety of reports on the preparation of nanostructures using EDTA-Na_2 were found in the literature involving α-Bi_2O_3,[30] YVO_4,[31] $CeVO_4$,[32] WO_3,[33] $LaVO_4$,[34] PbS[35] and ZnO[36] due to EDTA-Na_2 behavior of chelating, capping, and as a structure-directing effect. We suggested a possible control mechanism of Bi_2S_3 in regard to the

* E-mail: mikihan@ewha.ac.kr (Mi-Kyung Han), sjkim@ewha.ac.kr (Sung-Jin Kim), wooyoung@yonsei.ac.kr (Wooyoung Lee); [+] These authors equally contributed to this work.
Received January 2, 2013; accepted February 24, 2013; published online XXXX, 2013.

role of the capping and chelating agent, EDTA-Na_2. Our prepared products with variable morphologies via a hydrothermal process are still not reported in the literature and might be useful for a thermoelectric, electronic, and optoelectronic devices to create functional nanostructured materials.

Experimental

In a typical synthesis, 0.005 mol of $Bi(NO_3)_3$•$5H_2O$ was dissolved in 20 mL water. The mixture was added to a 50 mL Teflon lined stainless steel autoclave, which was filled with a 20 mL of Na_2S•$9H_2O$ (0.01 mol) aqueous solution. EDTA-Na_2 was added to the solution at four different molar ratio of EDTA-Na_2/Bi^{3+} (0, 0.3, 0.7, or 1) in order to control the morphology of Bi_2S_3 nanostructures. The autoclave was maintained at a temperature of 120 ℃ for 24 h. During the reaction, the solution was stirred by a stainless steel stirrer with a rotational speed of 50 r/min. After the reaction, the autoclave was naturally cooled to room temperature. The powder (yield about 80%) was collected by filtration, washed with deionized water, ethanol, and acetone several times and then dried at 60 ℃ for 12 h in a vacuum. The powder XRD patterns were collected on a Rigaku D/MAX X-ray (40 kV and 30 A) diffractometer with Cu Kα radiation (λ=1.54056 Å). The sample morphologies, fine structures, and SAED patterns were obtained by field emission transmission electron microscopy (FE-TEM) using a model 2100F apparatus (JEOL, Tokyo, Japan).

Results and Discussion

Figure 1 shows the XRD patterns of the final products. All diffraction peaks could be indexed to the pure orthorhombic phase of Bi_2S_3. The lattice constants calculated from the XRD pattern in Figures 1b−1e were about 11.151−11.171 Å, 11.301−11.331 Å, and 3.977−3.981 Å for the lattice parameter *a*, *b*, and *c*, respectively. The results showed good agreement with the JCPDS data (JCPDS 17-0320, *a*=11.149 Å, *b*=11.304 Å and *c*=3.981 Å). Peaks for bismuth, oxide, or other bismuth sulfide-oxide compounds did not appear in the diffraction patterns. From the XRD pattern, stacked nanorods, nanoplates, and nanoparticles (Figures 2c−2e) showed no significant deviation from that of calculated Bi_2S_3. Enhanced (120) peak intensities in the XRD analysis were observed for the nanorod. The relative differences of peak intensity denoted a preferred crystallographic orientation. The above results indicated that the [00l] or $[2\bar{h}k0]$ was the preferred orientation direction of the Bi_2S_3 nanostructure without EDTA-Na_2, but the preferred orientation plane disappeared by increasing the amount of EDTA-Na_2. We confirmed the preferred orientation direction of Bi_2S_3 nanorod by SAED pattern and HRTEM (Figure 2).

Figure 2 shows representative TEM images of Bi_2S_3

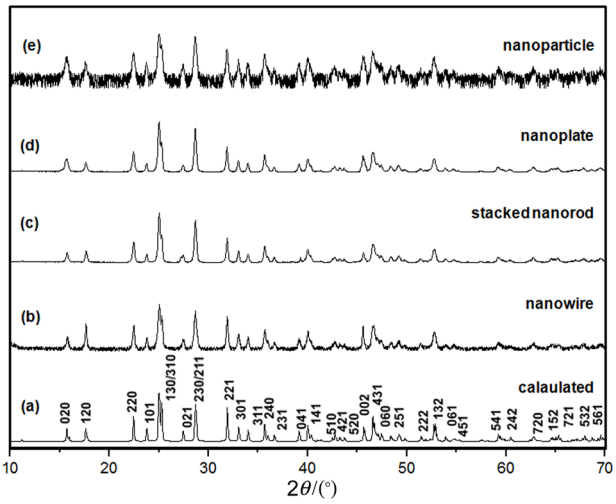

Figure 1 XRD patterns of powder products synthesized by hydrothermal method. (a) calculated Bi_2S_3, (b) without EDTA-Na_2, (c) EDTA-Na_2/Bi^{3+} molar ratio=0.3, (d) EDTA-Na_2/Bi^{3+} molar ratio=0.7, (e) EDTA-Na_2/Bi^{3+} molar ratio=1.

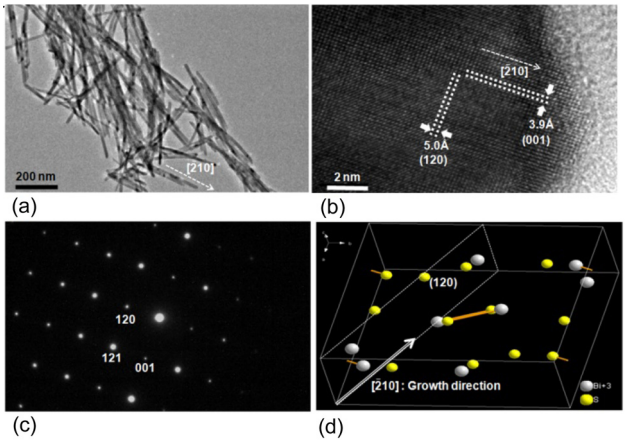

Figure 2 TEM and HRTEM images of powder product synthesized without EDTA-Na_2. (a) TEM image of Bi_2S_3 nanorod, (b) HRTEM image of Bi_2S_3 nanorod, (c) SAED pattern of Bi_2S_3 nanorod, (d) schematic diagram of the preferential growth direction.

nanorods prepared by the hydrothermal method without EDTA-Na_2. Nanorods displayed a diameter of 10−30 nm and a length of 400−900 nm (Figure 2a). The chemical reactions in the hydrothermal synthesis could be expressed as follows:

$$2Bi(NO_3)_3\,(aq) + 3Na_2S\,(aq) \rightarrow Bi_2S_3\,(s) + 6NaNO_3\,(aq)$$

$$Bi_2S_3 \text{ nucleation} \rightarrow Bi_2S_3 \text{ nanowires}$$

Bi^{3+} ions from $Bi(NO_3)_3$ react immediately with S^{2-} ions from Na_2S to form Bi_2S_3. The reaction solution changed color from clear to light gray immediately, indicating the formation of Bi_2S_3 nuclei. These freshly formed Bi_2S_3 nuclei in the solution grow into Bi_2S_3

nanowires. The HRTEM image shown in Figure 2b depicted the growth direction of a representative nanorod. The nanorod was a well crystallized single crystal, free from defects including a dislocation, a twin boundary, and a stacking fault. The distances of the lattice planes between two neighboring faces were estimated to be about 3.9 and 5.0 Å, which was exactly the same distances as that of interplanar distance between the (001) and (120) lattice planes of Bi_2S_3 crystal, respectively. Also, the SAD pattern in Figure 2c was a typical orthorhombic SAED pattern, which was indexed as the same plane of the HRTEM image. The (001) plane of SAD pattern in Figure 2c is a non-allowed reflection of Bi_2S_3 crystal structure. However, the forbidden reflection often appears due to breaks in crystal lattice symmetry, such as monatomic steps and kinks along the nanocrystal surface.[37] The nanowire in Figure 2 grew along the $[\bar{2}10]$ direction. This result confirmed that the preferential growth direction of the Bi_2S_3 nanorod was the $[\bar{2}10]$ direction, which was consistent with our XRD analysis and previous report for Bi_2S_3 nanoribbons.[9] In order to understand the growth of Bi_2S_3 nanorods, we needed to study its crystal structure. Figure 2d shows schematic diagram of the growth direction of the Bi_2S_3 unit cell.

Figure 3 shows the Bi_2S_3 nanorods formed at molar ratio of EDTA-Na_2/Bi^{3+}=0.3. TEM revealed that the stacked nanorod Bi_2S_3 possessed average edge lengths of about 0.3—0.7 μm. Figure 3b shows a magnified TEM image of stacked nanorod Bi_2S_3. The angle of the Bi_2S_3 stacked nanorod corner was about 90°, which matched the angle between the (120) and (001) lattice planes of Bi_2S_3 crystal structure. We found that the stacked nanorod Bi_2S_3 did not grow uni-directionally, but rather displayed two-way directional growth along the [001] and $[\bar{2}10]$ direction (Figures 3c and 3d). The morphology of the Bi_2S_3 nanostructure was changed as a result from a nanorod to a stacked nanorod due to the change of the growth direction from $[\bar{2}10]$ to [001] by the effect of EDTA-Na_2. In the case of the EDTA-Na_2/Bi^{3+} molar ratio of 0.7, Bi_2S_3 nanoplates were formed as shown in Figure 4a. Bi_2S_3 nanoplates had average edge lengths of about 300—500 nm. Figure 4b shows a typical HRTEM image of the Bi_2S_3 nanoplate, which was single crystalline as shown by the SAED pattern (Figure 4c). The distance of lattice planes was about 3.7 and 5.0 Å, which matched the distance between the $[\bar{2}20]$ and (120) lattice planes of Bi_2S_3, respectively. The angle between the $[\bar{2}20]$ and (120) planes is 72.2°. The corresponding SAED pattern was taken along the [001] zone axis. The SAED pattern was indexed in the same plane of the HRTEM image of Figure 4c. At the EDTA-Na_2/Bi^{3+} molar ratio of 1, very tiny Bi_2S_3 nanoparticles with irregular shape were formed. Figure 5a shows a representative Bi_2S_3 nanoparticle with average edge lengths of 10—20 nm and edge of the basal facets were not well defined. A representative HRTEM image shown in Figure 5b depicted the single crystal

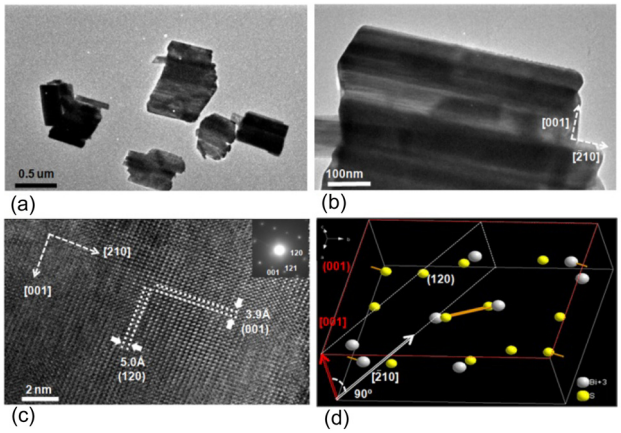

Figure 3 TEM and HRTEM images of powder product synthesized at EDTA-Na_2/Bi^{3+} molar ratio=0.3. (a) TEM image of the stacked nanorod Bi_2S_3, (b) Magnified TEM image of the stacked nanorod Bi_2S_3, (c) HRTEM image of the stacked nanorod Bi_2S_3 and SAED pattern (upper right), (d) Schematic diagram of the preferential and sub-optimal growth direction.

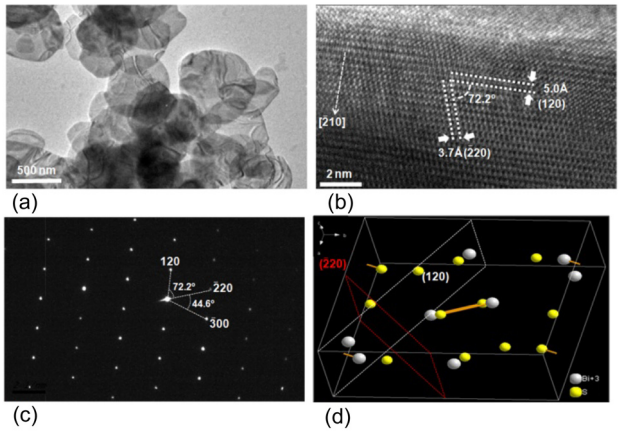

Figure 4 TEM and HRTEM images of powder product synthesized at EDTA-Na_2/Bi^{3+} molar ratio=0.7. (a) TEM image of Bi_2S_3 nanoplates, (b) HRTEM image of Bi_2S_3 nanoplate, (c) SAED pattern of Bi_2S_3 nanoplate, (d) schematic diagram of the related planes.

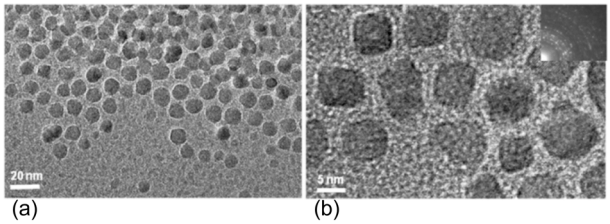

Figure 5 TEM and HRTEM images of powder product synthesized at EDTA-Na_2/Bi^{3+} molar ratio=1. (a) TEM image of Bi_2S_3 nanoparticles, (b) HRTEM image of Bi_2S_3 nanoparticles and SAED pattern (ring, upper right).

structure of Bi_2S_3 nanoparticles. The SAED pattern shows the random orientation of Bi_2S_3 nanoparticles, which agrees well with XRD results.

Many studies have reported that 2D growth model

for Bi_2S_3 crystal structure, such as nanosheet and nanoplate, can be attributed to the anisotropic Bi—S atom chains structure of Bi_2S_3 unit cell[38] or the splitting crystal growth process.[39] In our work, in order to understand the 2D growth of Bi_2S_3, we needed to know role of EDTA-Na_2. EDTA-Na_2 binds to Bi^{3+} ions through its two amines and four carboxylates.[40] In the absence of EDTA-Na_2, Bi_2S_3 nanorods were formed along the $[\bar{2}20]$ direction due to the intermolecular attraction between Bi and S atoms. However, in the presence of EDTA-Na_2/Bi^{3+} molar ratio of 0.3 and 0.7, the 1D growth of the Bi_2S_3 nanostructures was prohibited and instead formed 2D growth like a nanoplate and a stacked nanorod. This remarkable change shows that EDTA-Na_2 plays an important role in the morphology evolution. We propose that the formation of the 2D growth may result from the capping of Bi^{3+} ions with the EDTA-Na_2 in the (120) plane, which gives rise to a prohibition of crystal growth along the $[\bar{2}10]$ axis and inducement of crystal growth along the [001] direction. A similar morphological change of ZnO from nanowire to stacking nanoplates was reported in the presence of citrate as a complex agent,[41] which plays a similar role of EDTA-Na_2 in our experiment. In the case of the EDTA-Na_2/Bi^{3+} molar ratio of 1, we propose that EDTA-Na_2 is fully prohibited to growth of Bi_2S_3 structure. In aqueous solution with EDTA-Na_2, EDTA-Na_2 and Bi^{3+} react as follows:

$$Bi^{3+} + EDTA^{4-} \rightarrow (BiEDTA)^{-}$$

$$(BiEDTA)^{-} \rightarrow Bi^{3+} + EDTA^{4-}$$

$$Bi^{3+} + S^{2-} \rightarrow Bi_2S_3$$

$$Bi_2S_3 \text{ nucleation} \rightarrow Bi_2S_3 \text{ growth}$$

EDTA-Na_2 and Bi^{3+} can form very stable ligand complex shown in the above reaction. The Bi^{3+} with EDTA-Na_2 complex in aqueous solution proceeds with spontaneous nucleation and produces a number of nucleation. Then, Bi_2S_3 growth proceeds at very low rate due to the EDTA-Na_2 complex. Therefore, only small Bi_2S_3 particles can be produced. In the case of the EDTA-Na_2/Bi^{3+} molar ratio of 0.3 and 0.7, the capping effect of EDTA-Na_2 is a more dominant factor than the chelating effect, which only affects the growth direction of Bi_2S_3 nanostructure. While the EDTA-Na_2/Bi^{3+} molar ratio increases by 1, the growth of Bi_2S_3 nanostructure is fully restrained, thereby indicating that the chelating effect of EDTA-Na_2 is more dominant.

Figure 6 shows a schematic diagram of the proposed formation mechanism of nanostructured Bi_2S_3 at different molar ratios of EDTA-Na_2/Bi^{3+}. In case of reaction without EDTA-Na_2, Bi_2S_3 nanorods grow preferentially along the $[\bar{2}10]$ direction. When the molar ratio of EDTA-Na_2/Bi^{3+} is increased to 0.3, the Bi_2S_3 nanostructure first grows along the $[\bar{2}10]$ direction, then grows along the [001] direction due to the capping effect of EDTA-Na_2. When the molar ratio of EDTA-Na_2/Bi^{3+}=0.7, Bi_2S_3 nanostructure apparently forms a nanoplate (Figure 6c). When the molar ratio of EDTA-Na/Bi^{3+}=1, only small Bi_2S_3 particles can be produced due to the chelating effect of EDTA-Na_2.

Conclusions

Bi_2S_3 nanorods, stacked nanorods, nanoplates, and nanoparticles are synthesized through a hydrothermal method only by varying of molar ratio of EDTA-Na_2/Bi^{3+}. The powder XRD measurements verified that Bi_2S_3 nanorods, stacked nanorods, nanoplates, and nanoparticles are the same orthorhombic structure. The Bi_2S_3 nanorods grow in the $[\bar{2}10]$ direction due to the

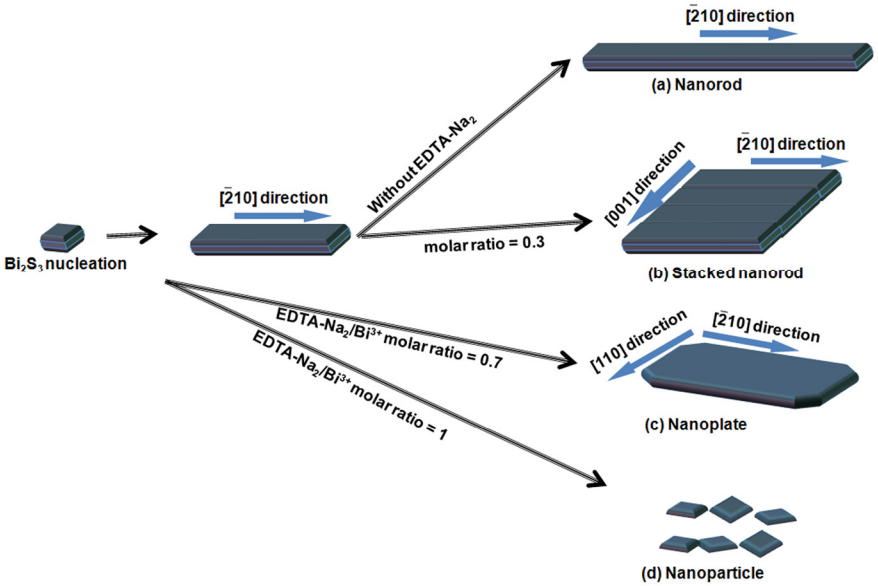

Figure 6 The schematic diagram of the formation of Bi_2S_3 nanostructures at different molar ratios of EDTA-Na_2/Bi^{3+}. (a) nanorod, (b) stacked nanorod, (c) nanoplate, and (d) nanoparticle.

intermolecular attraction between Bi and S atoms. At the molar ratio of EDTA-Na_2/Bi^{3+} = 0.3, stacked nanorod Bi_2S_3 grow along the *c* axis direction instead of the [$\bar{2}$10] direction. The change of Bi_2S_3 morphology results from the capping effect of Bi^{3+} ions with EDTA-Na_2, which partially blocks the preferential orientation direction and also drives growth in the suboptimal orientation direction. When the EDTA-Na/Bi^{3+} molar ratio = 1, the growth of Bi_2S_3 structure is not allowed due to the chelating effect of EDTA-Na_2.

Acknowledgement

W. Lee acknowledges for financial support by the Priority Research Centers Program (2009-0093823) and Pioneer Research Center Program (2010-0019313) through the National Research Foundation of Korea (NRF). This research was supported by Nano-Material Technology Development Program through the National Research Foundation of Korea (NRF) funded by the Ministry of Education, Science and Technology (20110030147), National Research Foundation of Korea Grant funded by the Korean Government (20120000651).

References

[1] Arivuoli, D.; Gnanam, F. D.; Ramasamy, P. *J. Mater. Sci. Lett.* **1988**, *7*, 711.
[2] Mahapatra, P. K.; Roy, C. B. *Sol. Cells* **1983**, *7*, 225.
[3] Nomura, R.; Kanaya, K.; Matsuda, H. *Bull. Chem. Soc. Jpn.* **1989**, *62*, 939.
[4] Boudjouk, P.; Remington Jr, M. P.; Grier, D. G.; Jarabek, B. R.; McCarthy, G. J. *Inorg. Chem.* **1998**, *37*, 35383.
[5] Zhang, W. X.; Yang, Z. H.; Huang, X. M.; Zhang, S. Y.; Yu, W. C.; Qian, Y. T.; Jia, Y. B.; Zhou, G. E.; Chen, L. *Solid State Commun.* **2001**, *143*, 119.
[6] Yu, S. H.; Qian, Y. T.; Shu, L.; Xie, Y.; Yang, L.; Wang, C. S. *Mater. Lett.* **1998**, *35*, 116.
[7] Sheng, G. Z.; Chen, D.; Tang, K. B.; Li, F. Q.; Qian, Y. T. *Chem. Phys. Lett.* **2003**, *370*, 334.
[8] Wang, D. B.; Shao, M. W.; Yu, D. B.; Li, G. P.; Qian, Y. T. *J. Cryst. Growth* **2002**, *243*, 331.
[9] Liu, Z.; Peng, S.; Xie, Q.; Hu, Z.; Yang, Y.; Zhang, S.; Qian, Y. *Adv. Mater.* **2003**, *15*, 936
[10] Wang, D.; Hao, C.; Zheng, W.; Ma, X.; Chu, D.; Peng, Q.; Li, Y. *Nano Res.* **2009**, *2*, 130.
[11] Liu, Z.; Liang, J.; Li, S.; Peng, S.; Qian, Y. *Chem. Eur. J.* **2004**, *10*, 634.
[12] Xiao, Y.; Cao, H.; Liu, K.; Zhang, S.; Chernow, V. *Nanotechnology* **2010**, *21*, 145601.
[13] Tang, C. J.; Zhang, Y. X.; Dou, X. C.; Li, G. H. *J. Cryst. Growth* **2010**, *312*, 692
[14] Thongtem, T.; Pilapong, C.; Kavinchan, J.; Phuruangrat, A.; Thongtem, S. *J. Alloys Compd.* **2010**, *500*, 195.
[15] Tao, X.-C.; Shao, M.-W. *Chin. J. Chem.* **2002**, *20*, 1121.
[16] Nomura, R.; Kanaya, K.; Matsuda, H. *Bull. Chem. Soc. Jpn.* **1989**, *62*, 939.
[17] Larionov, S. V.; Patrina, L. A.; Uskov, E. M. *Izv. Akad. Nauk SSSR, Ser. Fiz* **1979**, *3*, 94.
[18] Popov, V. N.; Kolodezev, A. B.; Safonov, V. P.; Soveshch, T. D. V. *Tekhnol., Protsessy, Appar. Kach. Prom. Lyuminoforov.* **1977**, 98.
[19] Cyganski, A.; Kobylecka, J. *Thermochim. Acta* **1981**, *45*, 65.
[20] Malakooti, R.; Cademartiri, L.; Akçakir, Y.; Petrov, S.; Migliori, A.; Ozin, G. A. *Adv. Mater.* **2006**, *18*, 2189.
[21] Wu, T.; Zhou, X.; Zhang, H.; Zhong, X. *Nano Res.* **2010**, *3*, 379.
[22] Li, L.; Sun, N.; Huang, Y.; Qin, Y.; Zhao, N.; Gao, J.; Li, M.; Zhou, H.; Qi, L. *Adv. Funct. Mater.* **2008**, *18*, 1194.
[23] Guo, C. F.; Cao, S.; Zhang, J.; Tang, H.; Guo, S.; Tian, Y.; Liu, Q. *J. Am. Chem. Soc.* **2011**, *133*, 8211.
[24] Song, C. X.; Wang, D. B.; Yang, T.; Hu, Z. S. *Cryst. Eng. Comm.* **2011**, *13*, 3087.
[25] Cademartiri, L.; Guerin, G.; Bishop, K. J. M.; Winnik, M. A.; Ozin, G. A. *J. Am. Chem. Soc.* **2012**, *134*, 9327.
[26] Bishop, K. J. M.; Wilmer, C. E.; Soh, S.; Grzybowski, B. A. *Small* **2009**, *5*, 1600.
[27] Nie, Z.; Petukhova, A.; Kumacheva, E. *Nat. Nanotechnol.* **2010**, *5*, 15.
[28] Gao, Y.; Tang, Z. *Small* **2011**, *7*, 2133.
[29] Jiang, J.; Gao, G.; Yu, R.; Qiu, G.; Liu, X. *Solid State Sci.* **2011**, *13*, 356.
[30] Xiong, Y.; Wu, M. Z.; Ye, J.; Chen, Q. W. *Mater. Lett.* **2008**, *62*, 1165.
[31] Ma, J.; Wu, Q. S.; Ding, Y. P. *Mater. Lett.* **2007**, *61*, 3616.
[32] Luo, F.; Jia, C. J.; Song, W.; You, L. P.; Yan, C. H. *Cryst. Growth Des.* **2005**, *5*, 137.
[33] Ha, J.-H.; Muralidharan, P.; Kim, D. K. *J. Alloys Compd.* **2009**, *475*, 446.
[34] Wang, N.; Chen, W.; Zhang, Q. F.; Dai, Y. *Mater. Lett.* **2008**, *62*, 109.
[35] Zhou, S. M.; Feng, Y. S.; Zhang, L. D. *J. Mater. Res.* **2003**, *18*, 5.
[36] Li, Z.; Fang, Y.; Peng, L.; Pan, D.; Wu, M. *Cryst. Res. Technol.* **2010**, *10*, 1083.
[37] Čomor, M. I.; Dramićanin, M. D.; Rakočević, Z.; Zec, S.; Nedeljković, J. M. *J. Mater. Sci. Lett.* **1998**, *17*, 1401.
[38] Ye, C.; Meng, G.; Jiang, Z.; Wang, Y.; Wang, G.; Zhang, L. *J. Am. Chem. Soc.* **2002**, *124*, 15180.
[39] Han, Q. F.; Feng, S.; Sun, Y.; Wang, X.; Yang, X. J.; Lu, L. D. *Mater. Lett.* **2009**, *63*, 1611.
[40] Kirchner, S. *Inorganic Syntheses*, McGraw-Hill, New York, **1957**.
[41] Cao, X. L.; Zeng, H. B.; Wang, M.; Xu, X. J.; Fang, M.; Ji, S. L.; Zhang, L. D. *J. Phys. Chem. C* **2008**, *112*, 5267.

(Zhao, X.)

